

Article

Modified Nonlocal Strain Gradient Elasticity for Nano-Rods and Application to Carbon Nanotubes

Raffaele Barretta ^{1,*} , Marko Čanadija ²  and Francesco Marotti de Sciarra ¹ 

¹ Department of Structures for Engineering and Architecture, University of Naples Federico II, via Claudio 21, 80125 Naples, Italy; marotti@unina.it

² Faculty of Engineering, University of Rijeka, Vukovarska 58, 51000 Rijeka, Croatia; marko.canadija@riteh.hr

* Correspondence: rabarret@unina.it

Received: 24 December 2018; Accepted: 30 January 2019; Published: 2 February 2019



Abstract: Nowadays, the modified nonlocal strain gradient theory provides a mathematically well-posed and technically reliable methodology to assess scale effects in inflected nano-structures. Such an approach is extended in this paper to investigate the extensional behavior of nano-rods. The considered integral elasticity model, involving axial force and strain fields, is conveniently shown to be equivalent to a nonlocal differential problem equipped with constitutive boundary conditions. Unlike treatments in the literature, no higher-order boundary conditions are required to close the nonlocal problem. Closed-form solutions of elastic nano-rods under selected loadings and kinematic boundary conditions are provided. As an innovative implication, Young's moduli of Single-Walled Carbon Nanotubes (SWCNT) were assessed and compared with predictions of Molecular Dynamics (MD). New benchmarks for numerical analyses were also detected.

Keywords: integral elasticity; modified nonlocal strain gradient elasticity; constitutive boundary conditions; higher-order boundary condition; nano-rods; carbon nanotubes; young modulus

1. Introduction

Components of Nano-Electro-Mechanical-Systems (NEMS), such as sensors and actuators, are usually modeled as nano-rods and nano-beams. It is well known that methods of local continuum mechanics cannot be adopted for such elements. Molecular Dynamics (MD) simulations are time-consuming and micro/nano-scaled experiments are usually difficult to implement. Hence, nonlocal continuum models have been developed for predicting the size-dependent mechanical behavior of nano-structures.

In the framework of nonlocal elasticity, Eringen's strain-driven differential model [1] has been widely adopted in the literature (see, e.g., [2–6]). It is worth noting that recent papers on the strain-driven nonlocal model [7–10] prove that, if the bending field is expressed as convolution of elastic curvature with an averaging kernel assuming an exponential expression, a solution of this problem exists only if the bending field satisfies constitutive boundary conditions. Accordingly, it is shown in [11] that the nonlocal elastostatic problem is ill-posed in all cases of applicative interest, as acknowledged in the literature (see, e.g., [12–18]). A modified version of the Eringen integral model is proposed in [19] and has been recently applied to inflected nanobeams in [20].

The gradient elasticity theory [21] assumes that a material at the nano-scale is modeled via gradient terms. Many works investigate the small-scale effects on the static and dynamic behaviors of rods, beams and plates and the effect of stiffness enhancement has been often reported in these strain gradient models (see, e.g., [22–26]).

Recently, the Eringen’s integral law [1] has been combined with the strain gradient elasticity in [27] to formulate a higher-order nonlocal theory, thus collecting nonlocal theory and strain gradient theory into a single model.

Using such a model, many contributions have been provided to model the size-dependent behavior of nano-rods and beams (see, e.g., [28–35]) and plates [36,37].

The procedure consists in considering the integral nonlocal gradient method for structural problems defined on bounded domains equivalent to a differential law of higher-order than the one of the classical local problem. Therefore, additional non-classical suitable boundary conditions must be added to solve the nonlocal strain gradient elastostatic problem.

To solve the problem, different choices have been followed in the literature. Two usual choices consist in imposing higher-order boundary conditions pertaining to the strain gradient theory, of kinematic type [38] or static type [39]. It is worth noting that the structural behavior is greatly influenced by such choices.

The nonlocal strain gradient theory with higher-order boundary conditions has been recently adopted in [40] to study nano-rods in tension. The closed-form solutions for predicting the axial displacement and the variation of the Young’s modulus have been derived for four different nano-rods differing by the choice of the higher-order boundary conditions. In particular, for each nano-rod, the nonlocal parameters have been set to match the variation of the Young’s modulus obtained by the MD simulations.

The choice of the higher-order boundary conditions is disputed in the literature and is considered an open question (see, e.g., [41]). In the context of nano-beams subjected to flexure, a recent contribution [42] provides a definite solution to this issue. In fact, the non-classical boundary conditions to be imposed to solve the elastostatic problem of nonlocal strain gradient inflected nano-beams are given by constitutive boundary conditions (CBC) that naturally follow from the nonlocal strain gradient integral model. The consistent nonlocal strain gradient strategy has been successfully applied to free vibrations of nano-beams in [43].

In the present paper, the structural behavior of nano-rods in tension is formulated in the framework of the modified nonlocal strain gradient (NSG) theory. The expressions of the CBC for nano-rods are explicitly provided and it is shown that no unmotivated higher-order boundary conditions have to be prescribed to solve the nonlocal structural problem.

In addition, the variation of the Young’s modulus provided by MD simulations is recovered based on the NSG model for nano-rods developed in the present paper. In particular, carbon nanotubes are effectively described by NSG nano-rods with the usual boundary conditions, that is clamped at the one end and with a tensile force at the other end. As illustrated in Appendix A, the same result is obtained if a doubly-clamped nano-rod with an imposed axial displacement at one end is considered.

Finally, numerical analyses are presented as benchmark examples for applications and experimental tests on nonlocal nano-rods.

2. Modified Nonlocal Strain Gradient Law for Rods

Let us consider a functionally graded (FG) straight nano-rod of length L , the x -coordinate is taken along the length of the nano-rod with the y -coordinate along the thickness and the z -coordinate along the width of the nano-rod. The local Young’s modulus E of the FG nano-rod continuously changes in the thickness direction y , so that the Young’s elastic modulus at the point y is $E(y)$ and the elastic area is $A_E = \int_{\Omega} E(y) dA$, being Ω the nano-rod cross-section.

In the modified nonlocal strain gradient (NSG) model for FG nano-rods, the axial force N is defined in terms of elastic axial strain ε_{el} and of its derivative $\partial_x \varepsilon_{el}$ is [27]

$$\begin{aligned}
 N(x, \lambda_0, \lambda_1, l) &= (\phi_0 * (A_E \varepsilon_{el}))(x, \lambda_0) - l^2 \partial_x (\phi_1 * (A_E \partial_x \varepsilon_{el}))(x, \lambda_1) \\
 &= \int_0^L \phi_0(x - \xi, \lambda_0) (A_E \varepsilon_{el})(\xi) d\xi - l^2 \partial_x \int_0^L \phi_1(x - \xi, \lambda_1) (A_E \partial_{\xi} \varepsilon_{el})(\xi) d\xi.
 \end{aligned}
 \tag{1}$$

The smoothing kernels ϕ_0 and ϕ_1 depend on two non-dimensional nonlocal parameters $\lambda_0 > 0$ and $\lambda_1 > 0$. The scale parameter $l > 0$, characteristic of the strain gradient elasticity [21], was subsequently introduced in [27] to make dimensionally homogeneous the convolutions in Equation (1) and to describe the importance of higher-order strain gradient fields.

Following [27,38], we consider that the nonlocal parameters are coincident, i.e., $\lambda := \lambda_0 = \lambda_1$, and the kernels ϕ_0 and ϕ_1 are coincident with the bi-exponential averaging function given by

$$\phi(x, L_c) = \frac{1}{2L_c} \exp\left(-\frac{|x|}{L_c}\right), \tag{2}$$

being $L_c = \lambda L$ the characteristic length of Eringen nonlocal elasticity. The kernel (Equation (2)) fulfills positivity, symmetry, normalization and impulsivity [42].

Introducing the following fields

$$\begin{aligned} N_0(x, L_c) &= \int_0^L \phi(x - \xi, L_c) (A_E \varepsilon_{el})(\xi) d\xi \\ N_1(x, L_c, l) &= l^2 \int_0^L \phi(x - \xi, L_c) (A_E \partial_\xi \varepsilon_{el})(\xi) d\xi, \end{aligned} \tag{3}$$

the modified nonlocal strain gradient elastic law (Equation (1)) can be rewritten as

$$N(x, L_c, l) = N_0(x, L_c) - \partial_x N_1(x, L_c, l). \tag{4}$$

As proven in the next proposition, the modified nonlocal strain gradient integral relation (Equation (4)) for FG nano-rods is equivalent to a suitable differential law with constitutive boundary conditions.

Proposition 1 (Constitutive equivalence for FG nano-rods). *The modified nonlocal strain gradient constitutive law (Equation (4)) equipped with the bi-exponential kernel (Equation (2))*

$$N(x, L_c, l) = N_0(x, L_c) - \partial_x N_1(x, L_c, l), \tag{5}$$

with $x \in [0, L]$, is equivalent to the differential relation

$$(A_E \cdot \varepsilon_{el})(x) - l^2 \partial_x^2 (A_E \cdot \varepsilon_{el})(x) = N(x, L_c, l) - L_c^2 \partial_x^2 N(x, L_c, l) \tag{6}$$

subject to the following two constitutive boundary conditions (CBC)

$$\begin{cases} \partial_x N(x, L_c, l)|_{x=0} = \frac{1}{L_c} N(0, L_c, l) + \frac{l^2}{L_c^2} \partial_x (A_E \varepsilon_{el})(x)|_{x=0} \\ \partial_x N(x, L_c, l)|_{x=L} = -\frac{1}{L_c} N(L, L_c, l) + \frac{l^2}{L_c^2} \partial_x (A_E \varepsilon_{el})(x)|_{x=L}. \end{cases} \tag{7}$$

Proof. Since the bi-exponential averaging function is given by

$$\phi(x, L_c) = \frac{1}{2L_c} \exp\left(-\frac{|x|}{L_c}\right), \tag{8}$$

a direct evaluation provides the first derivative of the convolutions (Equation (3))

$$\begin{aligned} \partial_x N_0(x, L_c) &= \frac{1}{L_c} \left[\int_x^L \phi(x - \zeta, L_c) (A_E \varepsilon_{el})(\zeta) d\zeta + \right. \\ &\quad \left. - \int_0^x \phi(x - \zeta, L_c) (A_E \varepsilon_{el})(\zeta) d\zeta \right] \\ \partial_x N_1(x, L_c, l) &= \frac{l^2}{L_c} \left[\int_x^L \phi(x - \zeta, L_c) \partial_{\zeta} (A_E \varepsilon_{el})(\zeta) d\zeta + \right. \\ &\quad \left. - \int_0^x \phi(x - \zeta, L_c) \partial_{\zeta} (A_E \varepsilon_{el})(\zeta) d\zeta \right]. \end{aligned} \tag{9}$$

The second derivative of the convolutions (Equation (3)) follows from Equation (9) using Equation (3) to get

$$\begin{aligned} \partial_x^2 N_0(x, L_c) &= \frac{1}{L_c^2} \left[l^2 \int_0^L \phi(x - \zeta, L_c) (A_E \varepsilon_{el})(\zeta) d\zeta + \right. \\ &\quad \left. - (A_E \varepsilon_{el})(x) \right] = \frac{1}{L_c^2} [N_0(x, L_c) - (A_E \varepsilon_{el})(x)] \\ \partial_x^2 N_1(x, L_c, l) &= \frac{l^2}{L_c^2} \left[\int_0^L \phi(x - \zeta, L_c) \partial_{\zeta}^2 (A_E \varepsilon_{el})(\zeta) d\zeta + \right. \\ &\quad \left. - \partial_x (A_E \varepsilon_{el})(x) \right] = \\ &= \frac{1}{L_c^2} [N_1(x, L_c, l) - l^2 \partial_x (A_E \varepsilon_{el})(x)]. \end{aligned} \tag{10}$$

Subtracting the third derivative of Equation (9)₂ from Equation (9)₁, it turns out to be

$$\begin{aligned} \partial_x^2 N_0(x, L_c) - \partial_x^3 N_1(x, L_c, l) &= \\ &= \frac{1}{L_c^2} [N_0(x, L_c) - (A_E \varepsilon_{el})(x)] + \\ &\quad - \frac{1}{L_c^2} [\partial_x N_1(x, L_c, l) - l^2 \partial_x^2 (A_E \varepsilon_{el})(x)] \end{aligned} \tag{11}$$

so that, recalling Equation (5) and rearranging the terms, we have

$$\begin{aligned} \partial_x^2 N(x, L_c, l) &= \partial_x^2 N_0(x, L_c) - \partial_x^3 N_1(x, L_c, l) = \\ &= \frac{1}{L_c^2} [N_0(x, L_c) - \partial_x N_1(x, L_c, l)] - \frac{1}{L_c^2} (A_E \varepsilon_{el})(x) + \frac{l^2}{L_c^2} \partial_x^2 (A_E \varepsilon_{el})(x) \end{aligned} \tag{12}$$

and Equation (6) is recovered.

The CBC in Equation (7) can be recovered as follows.

Using Equation (9)₂, Equation (5) can be rewritten in the form

$$\begin{aligned} N(x, L_c, l) &= N_0(x, L_c) - \frac{l^2}{L_c} \left[\int_x^L \phi(x - \zeta, L_c) \partial_{\zeta} (A_E \varepsilon_{el})(\zeta) d\zeta + \right. \\ &\quad \left. - \int_0^x \phi(x - \zeta, L_c) \partial_{\zeta} (A_E \varepsilon_{el})(\zeta) d\zeta \right] \end{aligned} \tag{13}$$

and using Equations (9)₁ and (7)₂, the first derivative of Equation (5) becomes

$$\begin{aligned} \partial_x N(x, L_c, l) &= \frac{1}{L_c} \left[\int_x^L \phi(x - \zeta, L_c) (A_E \varepsilon_{el})(\zeta) d\zeta + \right. \\ &\quad \left. - \int_0^x \phi(x - \zeta, L_c) (A_E \varepsilon_{el})(\zeta) d\zeta \right] + \\ &\quad - \frac{1}{L_c^2} [N_1(x, L_c, l) + l^2 \partial_x (A_E \varepsilon_{el})(x)]. \end{aligned} \tag{14}$$

The CBC (Equation (7)) of modified nonlocal strain gradient nano-rods follows by evaluating Equations (13) and (14) at nano-rod boundary points $x = 0$ and $x = L$. In fact, we have at $x = 0$

$$\begin{cases} N(0, L_c, l) = N_0(0, L_c) - \frac{l^2}{L_c} \left[\int_0^L \phi(-\xi, L_c) \partial_{\xi} (A_E \varepsilon_{el})(\xi) d\xi \right] \\ \partial_x N(x, L_c, l)|_{x=0} = \frac{1}{L_c} \left[\int_0^L \phi(-\xi, L_c) (A_E \cdot \varepsilon_{el})(\xi) d\xi \right] + \\ - \frac{1}{L_c^2} [N_1(0, L_c, l) + l^2 \partial_x (A_E \varepsilon_{el})(x)|_{x=0}] \end{cases} \quad (15)$$

so that Equation (15) provides the relations

$$\begin{cases} N(0, L_c, l) = N_0(0, L_c) - \frac{1}{L_c} N_1(0, L_c, l) \\ \partial_x N(0, L_c, l) = \frac{1}{L_c} N_0(0, L_c) - \frac{1}{L_c^2} N_1(0, L_c, l) + \frac{l^2}{L_c^2} \partial_x (A_E \varepsilon_{el})(x)|_{x=0} \end{cases} \quad (16)$$

and the CBC in Equation (7)₁ is recovered. Analogously, setting $x = L$ in Equation (14), we get

$$\begin{cases} N(L, L_c, l) = N_0(L, L_c) + \frac{l^2}{L_c} \left[\int_0^L \phi(L - \xi, L_c) \partial_{\xi} (A_E \varepsilon_{el})(\xi) d\xi \right] \\ \partial_x N(x, L_c, l)|_{x=L} = -\frac{1}{L_c} \left[\int_0^L \phi(L - \xi, L_c) (A_E \varepsilon_{el})(\xi) d\xi \right] + \\ - \frac{1}{L_c^2} [N_1(L, L_c, l) + l^2 \partial_x (A_E \varepsilon_{el})(x)|_{x=L}] \end{cases} \quad (17)$$

so that Equation (17) provides the relations

$$\begin{cases} N(L, L_c, l) = N_0(L, L_c) + \frac{1}{L_c} N_1(L, L_c, l) \\ \partial_x N(x, L_c, l)|_{x=L} = -\frac{1}{L_c} N_0(L, L_c) - \frac{1}{L_c^2} N_1(L, L_c, l) + \frac{l^2}{L_c^2} \partial_x (A_E \varepsilon_{el})(x)|_{x=L} \end{cases} \quad (18)$$

and the CBC in Equation (7)₂ is recovered. Conversely, sufficient condition can be inferred from the uniqueness of the solution of Equation (6) consequent to the fact that the associated homogeneous equations

$$\begin{cases} (A_E \varepsilon_{el})(x) - l^2 \partial_x^2 (A_E \varepsilon_{el})(x) = 0 \\ N(x, L_c, l) - L_c^2 \partial_x^2 N(x, L_c, l) = 0 \end{cases} \quad (19)$$

admit only the trivial solution under the homogeneous boundary conditions

$$\begin{cases} \partial_x (A_E \varepsilon_{el})(x)|_{x=0} = 0 \\ \partial_x (A_E \varepsilon_{el})(x)|_{x=L} = 0 \end{cases} \quad (20)$$

$$\begin{cases} \partial_x N(x, L_c, l)|_{x=0} = \frac{1}{L_c} N(0, L_c, l) \\ \partial_x N(x, L_c, l)|_{x=L} = -\frac{1}{L_c} N(L, L_c, l) \end{cases} \quad (21)$$

for (19)₁ and for (19)₂ respectively. \square

3. Elastic Equilibrium Problem

Let us consider a FG nano-rod subject to a distributed axial load $q(x)$ per unit length in the interval $[0, L]$ and to concentrated axial forces \mathcal{F} at the end cross-sections $x = 0$ and $x = L$.

Differential condition of equilibrium can be written as

$$\partial_x N(x, L_c, l) = -q(x) \tag{22}$$

with the boundary conditions $N(x, L_c, l) = \mp \mathcal{F}$ at $x = 0$ and $x = L$.

The axial displacement at the abscissa x along the nano-rod axis is denoted by $u(x)$ and the kinematically compatible axial strain has the form

$$\varepsilon(x) = \partial_x u(x). \tag{23}$$

In the sequel, elastic ε_{el} and kinematically compatible ε strains are assumed to be coincident.

Exact solutions according to the proposed modified nonlocal strain gradient (NSG) model for FG nano-rods can be performed by the following steps.

- **Step 1:** Solve the equilibrium Equation (22) to get the expression of the axial force

$$N(x, L_c, l) = -\int_0^x q(s) ds + a_1. \tag{24}$$

- **Step 2:** Solve the second-order differential Equation (6) in the form

$$\begin{aligned} (A_E \varepsilon_{el})(x) - l^2 \partial_x^2 (A_E \varepsilon_{el})(x) &= \\ &= -\int_0^x q(s) ds + a_1 + L_c^2 \partial_x q(x) \end{aligned} \tag{25}$$

obtaining the expression of the elastic axial strain ε_{el} of the nano-rod in terms of three integration constants (a_1, a_2 , and a_3) to be determined.

- **Step 3:** Solve the first-order differential in Equation (23) in terms of the axial displacement u of the nano-rod to get the expression of u in terms of four integration constants (a_1, a_2, a_3 , and a_4) to be determined.
- **Step 4:** Determine the four integration constants (a_1, a_2, a_3 , and a_4) by imposing the two CBC given by Equation (7) in terms of the axial displacement u

$$\begin{cases} -q(0) = \frac{1}{L_c} a_1 + \frac{l^2}{L_c^2} A_E \partial_x^2 u(x)|_{x=0} \\ -q(L) = \frac{1}{L_c} \left(\int_0^L q(s) ds - a_1 \right) + \frac{l^2}{L_c^2} A_E \partial_x^2 u(x)|_{x=L}. \end{cases} \tag{26}$$

and the two classical boundary conditions at the nano-rod end points $x = 0$ and $x = L$ by specifying

$$u \text{ or } N. \tag{27}$$

It is worth noting that, in statically determinate rods, the axial force N can be obtained by Equation (24) by imposing the classical static boundary conditions.

4. Closed-Form Solutions for FG Nano-Rods

Closed-form elastic solutions for FG nano-rods with a clamped end at $x = 0$ and a free end at $x = L$ and with both clamped ends are presented hereafter. The applied loads are a uniform load p , a concentrated force \mathcal{F} at $x = L$ (or an imposed axial displacement δ at $x = L$ for doubly-clamped rods). Kinematic and static boundary conditions are enforced to the FG nano-rod ends according to classical rod theory and, in addition, the constitutive boundary conditions Equation (26) are imposed according to the proposed NSG model. Hence, the axial displacement u can be recovered following Steps 1–4 in Section 3.

In the sequel, the abbreviations *CF* and *CC* stand for clamped-free and clamped-clamped, respectively. Moreover, let us assume that the elastic area A_E is constant along the nano-rod axis x .

For completeness sake, the FG nano-rod constraints, the considered applied load and the related boundary conditions are reported in Table 1.

Table 1. Fundamental schemes with corresponding boundary conditions.

FG Nano-Rod Constraints—Applied Load	Boundary Conditions	
	Classical	Constitutive
<i>CF</i> – \mathcal{F}	$u(0) = 0$	$\frac{F}{L_c} + \frac{l^2}{L_c^2} A_E \partial_x^2 u(x) _{x=0} = 0$
	$N(L) = \mathcal{F}$	$-\frac{F}{L_c} + \frac{l^2}{L_c^2} A_E \partial_x^2 u(x) _{x=L} = 0$
<i>CF</i> – p	$u(0) = 0$	$\frac{pL}{L_c} + \frac{l^2}{L_c^2} A_E \partial_x^2 u(x) _{x=0} = -p$
	$N(L) = 0$	$\frac{l^2}{L_c^2} A_E \partial_x^2 u(x) _{x=L} = -p$
<i>CC</i> – p	$u(0) = 0$	$\frac{a_1}{L_c} + \frac{l^2}{L_c^2} A_E \partial_x^2 u(x) _{x=0} = -p$
	$u(L) = 0$	$\frac{1}{L_c} (px - a_1) + \frac{l^2}{L_c^2} A_E \partial_x^2 u(x) _{x=L} = -p$
<i>CC</i> – δ	$u(0) = 0$	$\frac{a_1}{L_c} + \frac{l^2}{L_c^2} A_E \partial_x^2 u(x) _{x=0} = 0$
	$u(L) = \delta$	$-\frac{a_1}{L_c} + \frac{l^2}{L_c^2} A_E \partial_x^2 u(x) _{x=L} = 0$

To provide a non-dimensional analysis of FG nano-rods, the following non-dimensional variable ξ and the non-dimensional characteristic parameters λ and μ are adopted in the examples

$$\xi = \frac{x}{L}, \quad \lambda = \frac{L_c}{L}, \quad \mu = \frac{l}{L}. \tag{28}$$

The non-dimensional axial displacement \bar{u} depends on the kind of load applied to the nano-rod according to Table 2.

Table 2. Non-dimensional axial displacement \bar{u} in terms of the applied load.

Non-Dimensional Axial Displacement	Applied Load
$\bar{u} = u \frac{A_E}{pL^2}$	Uniform axial load p
$\bar{u} = u \frac{A_E}{\mathcal{F}L}$	Axial force \mathcal{F} at $x = L$
$\bar{u} = \frac{u}{\delta}$	Imposed axial displacement δ at $x = L$

4.1. Case I: CF FG Nano-Rod with a Concentrated Load at the Free End

Let us consider a FG nano-rod of length L with a clamped end at $x = 0$ and a free end at $x = L$ subject to a concentrated load \mathcal{F} at the free end.

Following the steps in Section 3, the axial force N can be evaluated by means of the equilibrium equation so that Equation (24), with the boundary condition $N(L) = \mathcal{F}$, yields $N(x) = \mathcal{F}$. For simplicity, we drop the dependence on the nonlocal characteristic parameters (L_c, l) . Then, the analytical solution of the NSG model for the FG nano-rod is obtained from the following nonlocal differential equation

$$A_E \partial_x u(x) - l^2 A_E \partial_x^3 u(x) = \mathcal{F} \tag{29}$$

under the CBC (Equation (26))

$$\left\{ \begin{array}{l} \frac{\mathcal{F}}{L_c} + \frac{l^2}{L_c^2} A_E \partial_x^2 u(x)|_{x=0} = 0 \\ -\frac{\mathcal{F}}{L_c} + \frac{l^2}{L_c^2} A_E \partial_x^2 u(x)|_{x=L} = 0 \end{array} \right. \tag{30}$$

and the kinematic boundary condition in Equation (27)

$$u(0) = 0. \tag{31}$$

Hence, the solution of the differential equation (Equation (29)) with the boundary conditions in Equations (30) and (31) provides the axial displacement

$$u(x) = u_e(x) + \frac{\mathcal{F}L_c}{A_E (e^{\frac{x}{L_c}} - 1)} e^{-\frac{x}{l}} (e^{\frac{x}{l}} - 1) (e^{\frac{x}{L_c}} + e^{\frac{x}{l}}) \tag{32}$$

where u_e is the rod axial displacement of the local model

$$u_e(x) = \frac{\mathcal{F}x}{A_E}. \tag{33}$$

The maximum displacement takes place at $x = L$ and can be obtained from Equation (32) setting $x = L$

$$u(L) = u_e(L) + \frac{2\mathcal{F}L_c}{A_E} = \frac{\mathcal{F}(L + 2L_c)}{A_E}. \tag{34}$$

The classical (local) displacement u_e of the FG nano-rod is provided by $L_c \rightarrow 0$. Moreover, the limit nano-rod displacement u_∞ for $l \rightarrow +\infty$ is given by

$$u_\infty(x) = u_e(x) + \frac{2\mathcal{F}L_c}{A_E L} x = \frac{\mathcal{F}(L + 2L_c)}{A_E L} x. \tag{35}$$

It is important to note that the NSG model for FG nano-rods exerts a softening effect, with respect to the local behavior, in terms of the nonlocal parameter L_c . It is of interest that the maximum displacement $u(L)$ of the NSG rod model does not depend on the gradient parameter l and the maximum axial displacement tends to the one of the classical (local) rod if $L_c \rightarrow 0$.

The effects of the non-dimensional characteristic parameters λ and μ on the elastic response of nano-rods are examined in Figures 1 and 2.

Figure 1a,b show the non-dimensional axial displacement \bar{u} in terms of the gradient non-dimensional parameter μ for $\lambda = 0.4$ and $\lambda = 0.8$, respectively. The local non-dimensional axial displacement \bar{u}_e is recovered by $\lambda \rightarrow 0^+$ and is reported with the dot dashed line. The limit non-dimensional axial displacement \bar{u}_∞ follows from Equation (35) and is reported with the dotted line in terms of the non-dimensional nonlocal parameter λ .

The comparison between nonlocal FG nano-rods and classical (local) FG rods in Figure 1 highlights the increment of the axial displacement \bar{u} due to the behavior of the nonlocal model. The parameter λ has the effect of increasing the axial displacement, i.e. a larger λ involves greater axial displacements \bar{u} for a given value of the non-dimensional gradient parameter μ .

Figure 2a shows the non-dimensional axial displacement \bar{u} of the FG nano-rod in terms of the nonlocal non-dimensional parameter λ for $\mu = 0.15$. The local non-dimensional axial displacement \bar{u}_e is recovered by $\lambda \rightarrow 0^+$ and is reported with the dot dashed line. The limit nano-rod non-dimensional axial displacement \bar{u}_∞ in terms of λ is plotted with the dotted line.

Figure 2b shows the non-dimensional axial displacement \bar{u} of the FG nano-rod in terms of the nonlocal non-dimensional parameter λ for $\mu = 0.15$ (thick lines) and $\mu = 0.30$ (dotted lines). The non-dimensional maximum axial displacement $\bar{u}(1)$ increases for increasing values of the nonlocal parameter λ and is independent of the non-dimensional gradient parameter μ . The limit nano-rod non-dimensional axial displacement \bar{u}_∞ is plotted with the black dotted line.

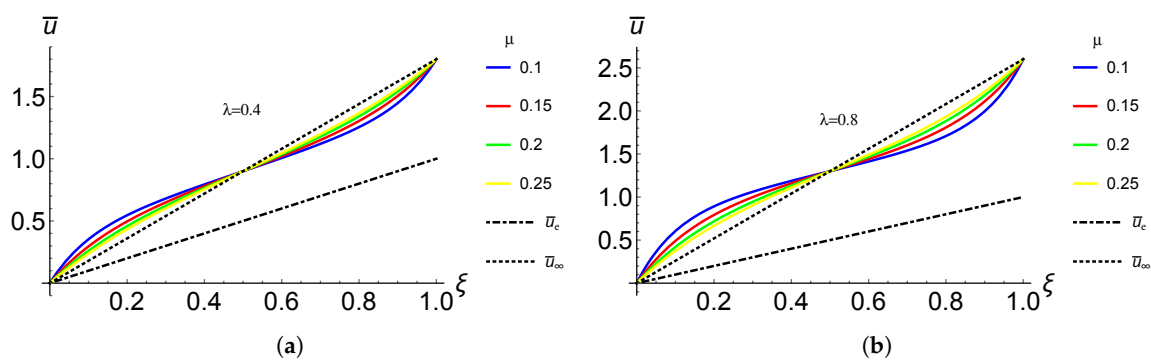


Figure 1. CF nano-rod with a concentrated load at the free end. Plot of the non-dimensional axial displacement \bar{u} , limit non-dimensional axial displacement \bar{u}_∞ (black dotted line) and local non-dimensional axial displacement \bar{u}_e (black dot dashed line) vs. the non-dimensional nano-rod axis for the gradient non-dimensional parameter μ in the set $\{0.10, 0.15, 0.20, 0.25\}$ and: (a) nonlocal non-dimensional parameter $\lambda = 0.4$; and (b) nonlocal non-dimensional parameter $\lambda = 0.8$.

The 3D plot of the non-dimensional maximum axial displacement $\bar{u}(1)$ for the proposed NSG method versus the non-dimensional characteristic parameters λ and μ is reported in Figure 3. The horizontal plane is the non-dimensional local maximum axial displacement $\bar{u}_e(1) = 1$.

The innovative nonlocal model exhibits a hardening behavior in terms of the non-dimensional characteristic parameter λ and the maximum axial displacement does not depend on the non-dimensional gradient parameter μ .

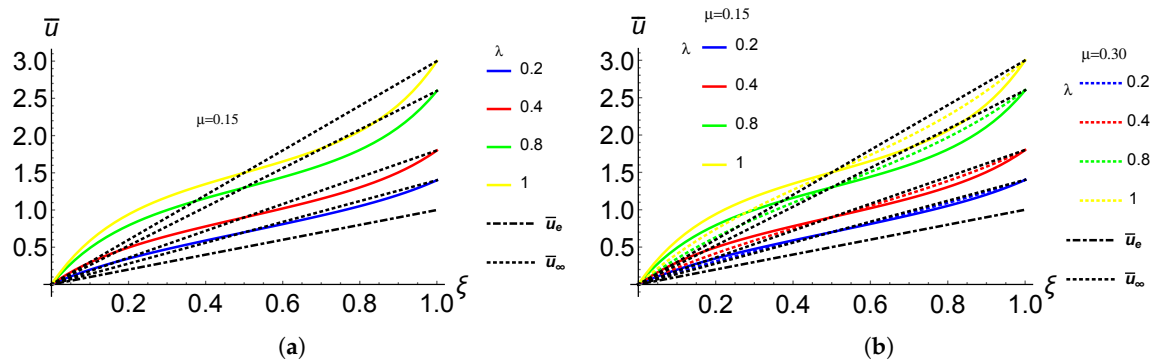


Figure 2. CF nano-rod with a concentrated load at the free end. Plot of the non-dimensional axial displacement \bar{u} , limit non-dimensional axial displacement \bar{u}_∞ (black dotted line) and local non-dimensional axial displacement \bar{u}_e (black dot dashed line) in terms of the nonlocal non-dimensional parameter λ in the set $\{0.2, 0.4, 0.8, 1.0\}$ and: (a) gradient non-dimensional parameter $\mu = 0.15$; and (b) gradient non-dimensional parameter μ in the set $\{0.15, 0.30\}$.

The nonlocal model coincides with the classical (local) model of rods for non-dimensional characteristic parameters λ tending to vanishing, i.e., and $\lambda \rightarrow 0^+$.

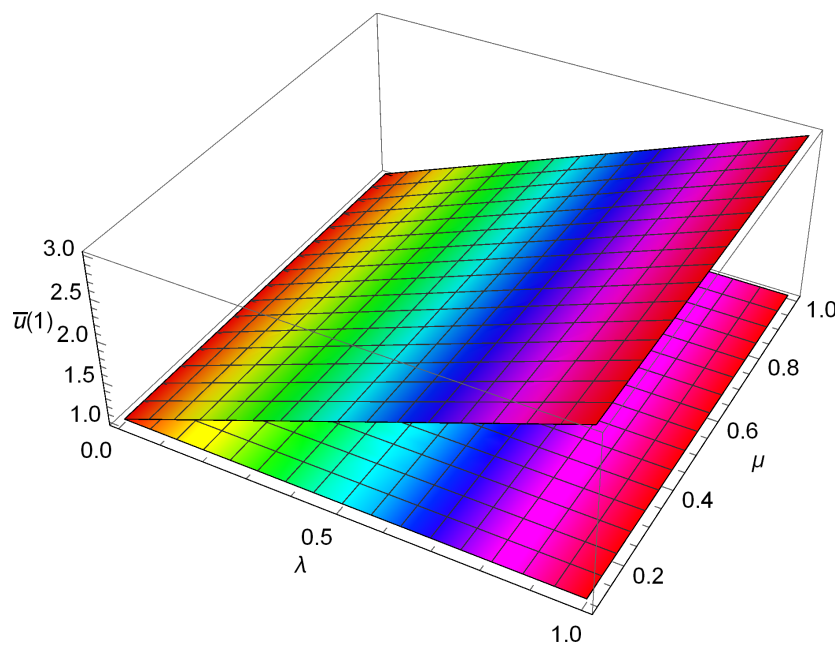


Figure 3. CF nano-rod with a concentrated load at the free end. 3D plot of the non-dimensional maximum axial displacement $\bar{u}(1)$ vs. the non-dimensional characteristic parameters λ and μ . The non-dimensional local maximum axial displacement $\bar{u}_e(1) = 1$ is the horizontal plane.

4.2. Reduced Young’s Modulus

In applications, the evaluation of the Young’s modulus of micro- and FG nano-rods is of great interest. Hence, we evaluate the reduced rigidity K_r from Equation (34) to get

$$K_r = \frac{L}{L + 2L_c} A_E. \tag{36}$$

Note that the classical rigidity $K_r = A_E$ can be recovered if $L_c \rightarrow 0$.

Using the reduced rigidity in Equation (36), the axial displacement of the modified nonlocal strain gradient model can be calculated by adopting the classical (local) analysis for rods. Let us consider a constant Young’s elastic modulus $E(y) = E$ so that the elastic area is $A_E = \int_{\Omega} E(y) dA = EA$. Hence, the reduced Young’s modulus E_r can be defined from Equation (36) as

$$E_r = \frac{L}{L + 2L_c} E \tag{37}$$

depending on the nonlocal parameter L_c . The upper bound of the nano-rod reduced Young’s modulus E_r for $L \rightarrow \infty$ is provided by the local Young’s modulus E . Analogously, for $L_c \rightarrow 0$, we recover the local Young’s modulus E and for $L_c \rightarrow +\infty$, the nano-rod reduced Young’s modulus tends to vanish.

To make a comparison, we considered the data presented in [40] for a SWCNT of armchair (10, 10). The diameter d of the SWCNT (n, m) can be calculated by

$$d = \frac{a}{\pi} \sqrt{3(n^2 + n \cdot m + m^2)} = 1.356 \text{ nm} \tag{38}$$

where the carbon–carbon bond length is $a = 0.142$ nm. The effective thickness of the considered SWCNT is $t = 0.34$ nm and the classical (local) Young’s modulus assumed in [40,44] is $E = 909.5$ GPa.

The Young’s modulus predicted by the MD simulations is reported in [40,44]. Note that the strain gradient elastic theory with high-order boundary conditions was adopted in [40] and the necessity to impose higher-order (non-classical) boundary conditions has the effect that the classical boundary conditions of the classical theory (such as free and clamped boundary conditions) may no longer be meaningful for the modified nonlocal strain gradient rod. As a result, following [28,35], one needs to take into account further boundary conditions involving higher-order stress and strain distributions. Accordingly, four nonlocal nano-rods are considered in [40], depending on the considered higher-order boundary conditions, and for each of them the small-scale parameters are set to match the results of the MD simulations.

On the contrary, the proposed NSG model has no higher-order boundary condition to add so that the classical definitions of external constraints must not be modified. Hence, a unique model of rod can be considered and a unique value of the nonlocal parameter has to be set to match the results of the MD simulations.

In Figure 4 the results provided by Equation (37) are plotted together with the MD data versus the SWCNT length. Upper and lower bounds of the nonlocal parameter $L_c = 0.04272$ nm and $L_c = 0.06942$ nm are reported in Figure 4a to include the values provided by the MD simulations. A good agreement between the Young’s modulus obtained by the NSG model and the MD results could be obtained by setting the nonlocal parameter $L_c = 0.0534$ nm, as shown in Figure 4b.

The NSG model provides values of the reduced Young’s modulus E_r tending to the classical (local) value E for increasing values of the SWCNT length L . On the contrary, the values of the MD simulations appear to be constant for values of the SWCNT’s length greater than 27 nm.

The small-scale effect on displacements can be clearly observed in Figure 5 where the non-dimensional maximum displacement $u(L)/L$, pertaining to the NSG model, is plotted versus the SWCNT’s length L for an applied force $F = 1$ nN and the nonlocal parameter L_c ranging in the set $\{0.04272, 0.0534, 0.06942\}$ nm. As can be seen, the small-scale effect on the displacement can be observed when the length of SWCNT is small and the small-scale effect increases for increasing values of the nonlocal parameter L_c . If $L \rightarrow +\infty$, the non-dimensional maximum displacement $u(L)/L$ tends to the corresponding local one $1/A_E = 7.59117 \times 10^{-4}$.

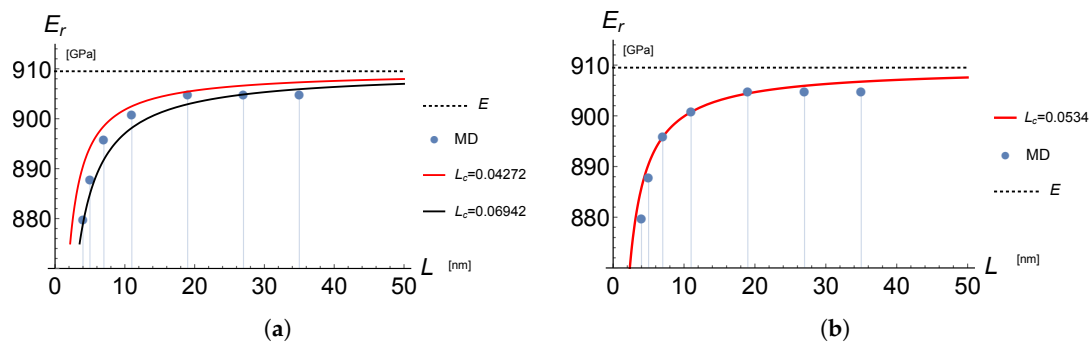


Figure 4. SWCNT of armchair (10, 10) having diameter $d = 1.356 \text{ nm}$, effective thickness $t = 0.34 \text{ nm}$ and classical (local) Young’s modulus $E = 909.5 \text{ GPa}$ simulated by a CF nano-rod with a concentrated load at the free end. (a) Plot the variation of the Young’s modulus obtained by the NSG method together with the MD data versus the SWCNT length. The upper bound is given for the nonlocal parameter $L_c = 0.04272 \text{ nm}$ and the lower bound is given for the nonlocal parameter $L_c = 0.06942 \text{ nm}$. (b) Variation of the Young’s modulus obtained by the NSG model and the MD data for the nonlocal parameter $L_c = 0.0534 \text{ nm}$.

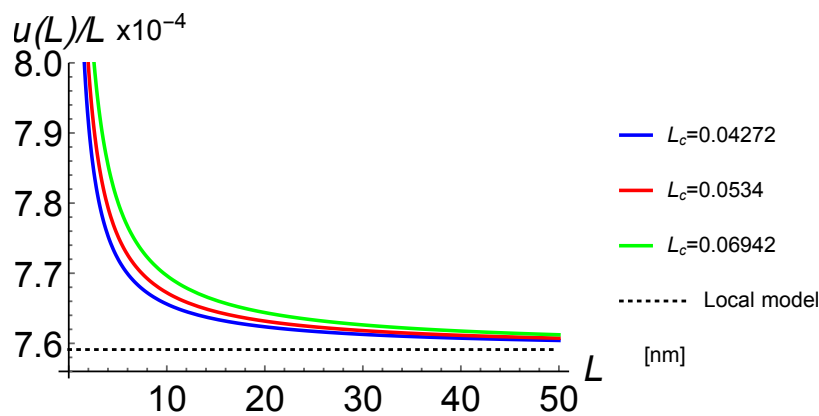


Figure 5. SWCNT of armchair (10, 10) having diameter $d = 1.356 \text{ nm}$, effective thickness $t = 0.34 \text{ nm}$ and classical (local) Young’s modulus $E = 909.5 \text{ GPa}$ simulated by a CF nano-rod with a concentrated load $F = 1 \text{ nN}$ at the free end. Plot of the non-dimensional maximum displacement $u(L)/L$ of the NSG model vs. the SWCNT’s length L for the nonlocal parameter L_c ranging in the set $\{0.04272, 0.0534, 0.06942\} \text{ nm}$. The non-dimensional local maximum displacement (black dotted line) is $1/A_E = 7.59117 \times 10^{-4}$.

In [45], a continuum mechanics model has been proposed to predict the effective wall thickness of a SWCNT and to calculate its Young’s modulus. The deformation of a central long SWCNT in a bundle of SWCNTs, subjected to an external pressure, has been considered in plane-strain and has been modeled as a thin ring with a mean radius R , thickness t in the radial direction and a unit width in the axial direction. Hence, it has been obtained that the radius of the nanotube is $R = 0.7066 \text{ nm}$ and the predicted thickness is $t = 0.0617 \text{ nm}$ so that the related Young’s modulus is $E = 4880 \text{ GPa}$. Considering the nonlocal parameter (dependent on the longitudinal atom spacing in armchair CNTs [46,47]) $L_c = 0.0534 \text{ nm}$ as previously calibrated by means of the MD data, the variation law of Young’s modulus obtained by the proposed NSG model for the SWCNT investigated in [45] is reported in Figure 6, with radius $R = 0.7066 \text{ nm}$, thickness $t = 0.0617 \text{ nm}$ and Young’s modulus $E = 4880 \text{ GPa}$. The NSG model provides values of the reduced Young’s modulus E_r tending to the value $E = 4880 \text{ GPa}$ for increasing values of the SWCNT length L .

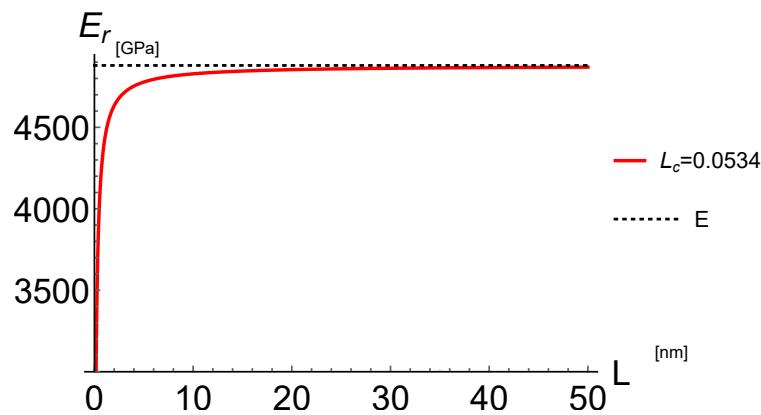


Figure 6. Plot the variation of the Young’s modulus obtained by the NSG method versus the SWCNT length for the nonlocal parameter $L_c = 0.0534$ nm simulated by a CF nano-rod with a concentrated load at the free end. The data of the SWCNT are: diameter $d = 1.4132$ nm, effective thickness $t = 0.0617$ nm and Young’s modulus $E = 4880$ GPa.

It is apparent that, for a nanotube with $L = 4$ nm, the reduced Young’s modulus is $E_r = 4753$ GPa, achieving 97.4% of the value of E . Hence, we can conclude that, for the SWCNT considered in [45], the variation of the Young’s modulus E_r is really small if the length of the SWCNT is greater than 4 nm. The small-scale effect on displacements is observed in Figure 7, in which the non-dimensional maximum displacement $u(L)/L$ of the NSG model is plotted versus the SWCNT’s length L for an applied force $F = 1$ nN and the nonlocal parameter L_c ranging in the set $(0.04272, 0.0534, 0.06942)$ nm. The small-scale effect on the displacement is apparent and the small-scale effect increases for increasing values of the nonlocal parameter L_c . The non-dimensional maximum displacement $u(L)/L$ tends to the corresponding local displacement $1/AE = 7.48069 \times 10^{-4}$ if L tends to $+\infty$.

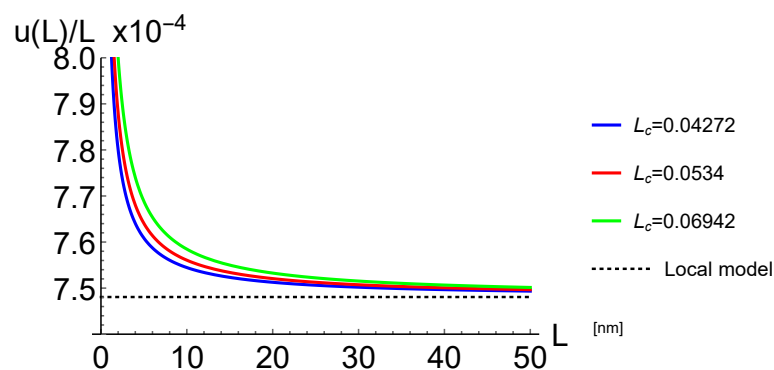


Figure 7. Plot of the non-dimensional maximum displacement $u(L)/L$ of the NSG model vs. the SWCNT’s length L for the nonlocal parameter L_c ranging in the set $(0.04272, 0.0534, 0.06942)$ nm. The non-dimensional local maximum displacement (black dotted line) is $1/AE = 7.48069 \times 10^{-4}$. The data of the SWCNT are: diameter $d = 1.4132$ nm, effective thickness $t = 0.0617$ nm and Young’s modulus $E = 4880$ GPa.

4.3. Case II: CF FG Nano-Rod Subject to a Uniformly Distributed Axial Load

Let us now consider a FG nano-rod with a clamped end at $x = 0$ and a free end at $x = L$ subject to a uniformly distributed axial load $q(x) = p$.

Following the steps reported in Section 3, the axial force N can be evaluated by means of the equilibrium equation so that Equation (24), with the boundary condition $N(L) = 0$, yields $N(x) =$

$p(L - x)$. Hence, the closed-form solution of the NSG model for the considered FG nano-rod is obtained by the following nonlocal differential equation

$$A_E \partial_x u(x) - l^2 A_E \partial_x^3 u(x) = p(L - x) \tag{39}$$

under the CBC in Equation (26)

$$\begin{cases} \frac{pL}{L_c} + \frac{l^2}{L_c^2} A_E \partial_x^2 u(x)|_{x=0} = -p \\ \frac{l^2}{L_c^2} A_E \partial_x^2 u(x)|_{x=L} = -p \end{cases} \tag{40}$$

and the classical boundary condition in Equation (27)

$$u(0) = 0. \tag{41}$$

Hence, the axial displacement is

$$u(x) = u_e(x) + \frac{p}{A_E \left(e^{\frac{2l}{L}} - 1 \right)} e^{-\frac{x}{l}} \left(e^{\frac{x}{l}} - 1 \right) \cdot \left[e^{\frac{l}{L}} (l^2 - L_c^2) + e^{\frac{L+x}{L}} (l^2 - L_c^2) + e^{\frac{2l}{L}} (-l^2 + LL_c + L_c^2) + e^{\frac{x}{L}} (-l^2 + LL_c + L_c^2) \right] \tag{42}$$

where u_e is the axial displacement of the local model

$$u_e(x) = \frac{px}{2A_E} (2L - x). \tag{43}$$

The maximum axial displacement of the CF FG nano-rod is attained at the free end $x = L$ and is given by

$$u(L) = u_e(L) + \frac{pLL_c}{A_E} = \frac{pL(L + 2L_c)}{2A_E}. \tag{44}$$

It is apparent from Equation (42) that the axial displacement u depends on the nonlocal parameters l and L_c . On the contrary, the maximum axial displacement $u(L)$ (see Equation (44)) is independent of the nonlocal gradient parameter l .

The limit maximum axial FG nano-rod displacement for the nonlocal parameter $L_c \rightarrow 0$ is given by the classical (local) displacement $u_e(L) = \frac{pL^2}{2A_E}$ of the FG nano-rod.

The non-dimensional axial displacement \bar{u} of the FG nano-rod versus the FG nano-rod non-dimensional length ξ is reported in Figure 8 in terms of the nonlocal non-dimensional parameter λ for $\mu = 0.15$ (thick lines) and $\mu = 0.30$ (dotted lines). The non-dimensional maximum axial displacement $\bar{u}(1)$ increases for increasing values of the nonlocal parameter λ and is independent of the non-dimensional gradient parameter μ . The limit FG nano-rod non-dimensional axial displacement for the non-dimensional nonlocal parameter λ tending to vanish is given by

$$\bar{u}_{lim}(\xi) = \frac{\left(-1 + e^{\frac{\xi}{\mu}} \right) \left(e^{\frac{\xi}{\mu}} - e^{\frac{1}{\mu}} \right)}{1 + e^{\frac{1}{\mu}}} \mu^2 e^{-\frac{\xi}{\mu}} - \frac{1}{2} (\xi - 2) \xi \tag{45}$$

and is reported with magenta thick line for $\mu = 0.15$ and dotted line for $\mu = 0.30$. Note that $\bar{u}_{lim}(1) = \bar{u}_e(1) = 0.5$.

The limit non-dimensional axial displacement \bar{u}_∞ for $\mu \rightarrow 0$ is obtained from Equation (42) and is given by

$$\bar{u}_\infty(\xi) = \left(\frac{1}{2} + \lambda\right) \xi. \tag{46}$$

The corresponding plot is reported with the black dotted line in Figure 8 for the considered values of the non-dimensional nonlocal parameter λ .

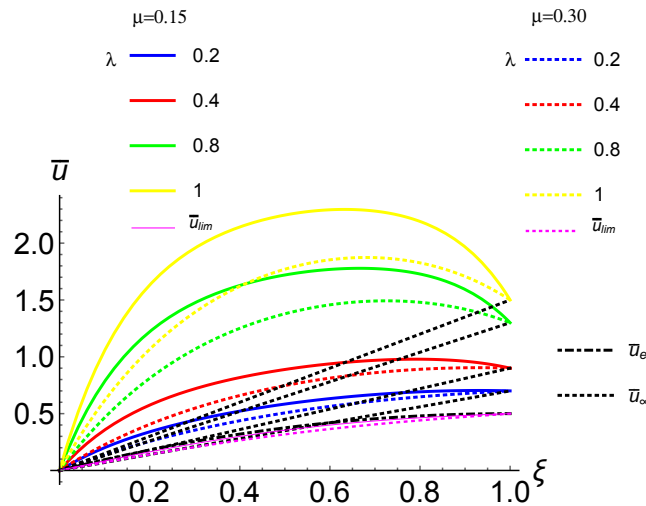


Figure 8. CF nano-rod with a uniformly distributed axial load. Plot of the non-dimensional axial displacement \bar{u} , limit non-dimensional axial displacement \bar{u}_∞ (black dotted line) and local non-dimensional axial displacement \bar{u}_e (black dot dashed line) vs. the nano-rod non-dimensional length ξ in terms of the nonlocal non-dimensional parameter λ in the set $\{0.2, 0.4, 0.8, 1.0\}$ and gradient non-dimensional parameter μ in the set $\{0.15, 0.30\}$.

4.4. Case III: CC FG Nano-Rod Subject to a Uniformly Distributed Axial Load

Let us consider a fully clamped FG nano-rod subject to a uniformly distributed axial load $q(x) = p$.

Following the steps reported in Section 3, the axial force is $N(x) = -px + a_1$ so that the analytical solution of the FG nano-rod is provided as

$$A_E \partial_x u(x) - l^2 A_E \partial_x^3 u(x) = -px + a_1 \tag{47}$$

under the CBC in Equation (26)

$$\begin{cases} \frac{a_1}{L_c} + \frac{l^2}{L_c^2} A_E \partial_x^2 u(x)|_{x=0} = -p \\ \frac{1}{L_c} (px - a_1) + \frac{l^2}{L_c^2} A_E \partial_x^2 u(x)|_{x=L} = -p \end{cases} \tag{48}$$

and the classical boundary condition in Equation (27)

$$\begin{cases} u(0) = 0 \\ u(L) = 0. \end{cases} \tag{49}$$

Hence, the axial displacement is

$$u(x) = u_e(x) + \frac{p}{2A_E (e^{\frac{l}{L_c}} + 1)} e^{-\frac{x}{L_c}} (e^{\frac{x}{L_c}} - 1) \cdot \left[(e^{\frac{x}{L_c}} - e^{\frac{l}{L_c}}) (2l^2 - LL_c - 2L_c^2) \right] \tag{50}$$

where u_e is the axial displacement of the local model

$$u_e(x) = \frac{px}{2A_E} (L - x). \tag{51}$$

Note that we have $a_1 = pL/2$ so that the axial force of the NSG method is $N(x) = p(L - 2x)/2$ and coincides to the local one.

The non-dimensional axial displacement \bar{u} of the FG nano-rod versus the FG nano-rod non-dimensional length ξ is reported in Figure 9 in terms of the nonlocal non-dimensional parameter λ for $\mu = 0.15$ (thick lines) and $\mu = 0.30$ (dotted lines). The non-dimensional midspan axial displacement $\bar{u}(1/2)$ increases for increasing values of the nonlocal parameter λ for a given μ . The limit FG nano-rod non-dimensional axial displacement for the non-dimensional nonlocal parameter λ tending to vanish follows from Equation (50)

$$\bar{u}_{lim}(\xi) = \frac{\left(-1 + e^{\frac{\xi}{\mu}}\right) \left(e^{\frac{\xi}{\mu}} - e^{\frac{1}{\mu}}\right)}{1 + e^{\frac{1}{\mu}}} \mu^2 e^{-\frac{\xi}{\mu}} - \frac{1}{2} (\xi - 1) \xi \tag{52}$$

and is reported with magenta thick line for $\mu = 0.15$ and dotted line for $\mu = 0.30$.

The limit non-dimensional axial displacement \bar{u}_∞ is obtained from Equation (50) for $\mu \rightarrow \infty$ and is the vanishing one, i.e., $\bar{u}_\infty(\xi) = 0$. The corresponding plot is reported with the black dotted line in Figure 9.

The 3D plot of the non-dimensional maximum axial displacement $\bar{u}(1/2)$ for the proposed NSG method versus the non-dimensional characteristic parameters λ and μ is reported in Figure 10. It is apparent that the NSG method stiffens or softens the nano-rod depending on the values of the non-dimensional nonlocal and gradient parameters (λ, μ) .

The cuts of the 3D plot for given values of the non-dimensional parameters λ and μ are provided in Figure 11. In particular, the plots of the non-dimensional maximum axial displacement $\bar{u}(1/2)$ for the NSG method versus the non-dimensional characteristic parameter λ for $\mu = 0.2$ and $\mu = 0.6$ are provided in Figure 11a. It is apparent that for $\mu = 0.2$ and $\lambda < 0.070156$ or $\mu = 0.6$ and $\lambda < 0.4$ the NSG model is stiffer than the local model and for $\mu = 0.2$ and $\lambda > 0.070156$ or $\mu = 0.6$ and $\lambda > 0.4$ the NSG model softens the nano-rod. The limit values of the non-dimensional maximum axial displacement $\bar{u}(1/2)$ for $\lambda \rightarrow 0^+$ are given by 0.0915228 for $\mu = 0.2$ and by 0.0281989 for $\mu = 0.6$.

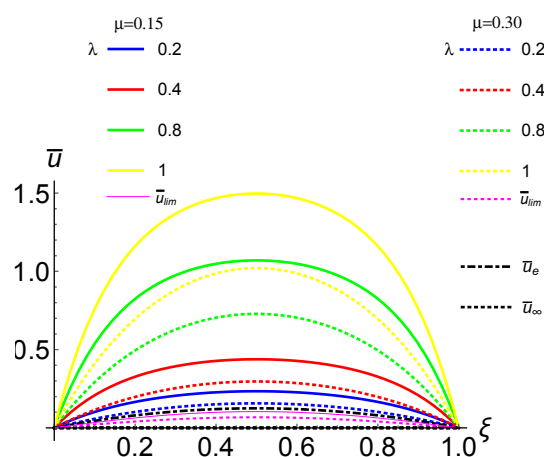


Figure 9. CC nano-rod subject to a uniformly distributed axial load. Plot of the non-dimensional axial displacement \bar{u} , limit non-dimensional axial displacement \bar{u}_∞ (black dotted line) and local non-dimensional axial displacement \bar{u}_e (black dot dashed line) vs. the nano-rod non-dimensional length ξ in terms of the nonlocal non-dimensional parameter λ in the set $\{0.2, 0.4, 0.8, 1.0\}$ and gradient non-dimensional parameter μ in the set $\{0.15, 0.30\}$.

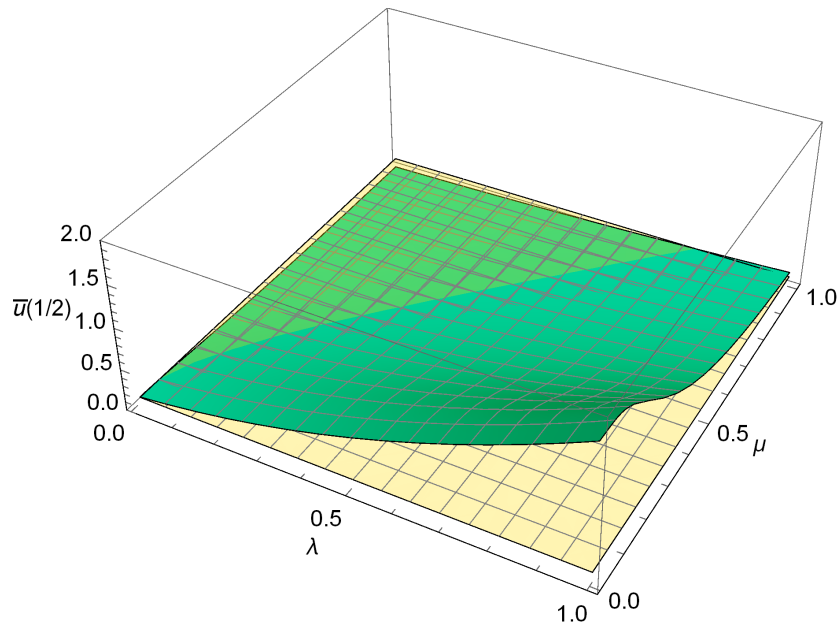


Figure 10. CC nano-rod subject to a uniformly distributed axial load. 3D plot of the non-dimensional maximum axial displacement $\bar{u}(1/2)$ vs. the non-dimensional characteristic parameters λ and μ . The non-dimensional local maximum axial displacement $\bar{u}_e(1/2) = 1/8 = 0.125$ is the horizontal plane.

The plots of the non-dimensional maximum axial displacement $\bar{u}(1/2)$ for the NSG method versus the non-dimensional characteristic parameter μ for $\lambda = 0.2$ and $\lambda = 0.6$ are provided in Figure 11b. It is immediate to note that for $\lambda = 0.2$ and $\mu < 0.374166$ or $\lambda = 0.6$ and $\mu < 0.812404$ the NSG model is stiffer than the local model and for $\lambda = 0.2$ and $\mu > 0.374166$ or $\lambda = 0.6$ and $\mu > 0.812404$ the NSG model softens the nano-rod. The limit values of the non-dimensional maximum axial displacement $\bar{u}(1/2)$ for $\mu \rightarrow 0^+$ are given by 0.265 for $\lambda = 0.2$ and by 0.785 for $\lambda = 0.6$.

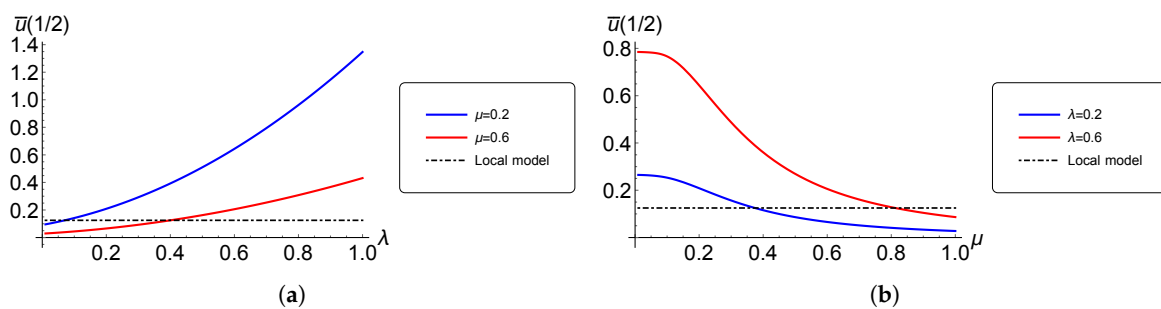


Figure 11. CC nano-rod subject to a uniformly distributed axial load. (a) The non-dimensional maximum axial displacement $\bar{u}(1/2)$ for the NSG method vs. the non-dimensional characteristic parameter λ for $\mu = 0.2$ and $\mu = 0.6$. (b) The non-dimensional maximum axial displacement $\bar{u}(1/2)$ for the NSG method vs. the non-dimensional characteristic parameters μ for $\lambda = 0.2$ and $\lambda = 0.6$.

Finally, a standard numerical analysis of Equation (50) shows that the non-dimensional maximum axial displacement $\bar{u}(1/2)$ for the proposed NSG method is attained at the midspan and is reported in Table 3 in terms of the non-dimensional nonlocal parameter λ and gradient parameter μ . It worth noting that the maximum displacement is attained at the midspan $\xi = 1/2$ of the FG nano-rod independent of the values of λ and μ . The non-dimensional maximum axial displacement of the classical (local) model is $\bar{u}_e(1/2) = 1/8 = 0.125$. Accordingly, the non-dimensional maximum axial displacements $\bar{u}(1/2)$ in terms of the pairs (λ, μ) , which are less than the non-dimensional maximum classical axial displacements $\bar{u}_e(1/2) = 0.125$ of the FG nano-rod, are reported in *italic* in Table 3.

Hence, the italic values of the non-dimensional maximum axial displacement $\bar{u}(1/2)$ of the NSG method are smaller than the one of the classical (local) model, thus Table 3 allows one to identify the corresponding pairs (λ, μ) having the effect of stiffen or soften the FG nano-rod with respect the classical (local) behavior.

Table 3. Non-dimensional maximum axial displacement $\bar{u}(1/2)$ for the proposed NSG method in terms of the non-dimensional parameters λ and μ .

$\lambda \setminus \mu$	0.1	0.2	0.3	0.4	0.5
0.1	0.1743260	0.1417390	0.1059420	0.0779542	0.0581303
0.2	0.2532480	0.2086930	0.1567630	0.1155910	0.0862860
0.3	0.3519010	0.2923860	0.2202890	0.1626370	0.1214810
0.4	0.4702840	0.3928170	0.2965200	0.2190920	0.1637140
0.5	0.6083970	0.5099870	0.3854570	0.2849560	0.2129860
0.6	0.7662410	0.6438960	0.4870980	0.3602290	0.2692980
0.7	0.9438160	0.7945430	0.6014450	0.4449110	0.3326480
0.8	1.1411200	0.9619290	0.7284970	0.5390030	0.4030370
0.9	1.3581600	1.1460500	0.8682550	0.6425040	0.4804650
1.0	1.5949200	1.3469200	1.0207200	0.7554140	0.5649320
$\lambda \setminus \mu$	0.6	0.7	0.8	0.9	1.0
0.1	0.0443324	0.0346164	0.0276280	0.0224832	0.0186098
0.2	0.0658438	0.0514320	0.0410586	0.0334183	0.0276642
0.3	0.0927330	0.0724514	0.0578469	0.0470872	0.0389824
0.4	0.1250000	0.0976747	0.0779928	0.0634899	0.0525641
0.5	0.1626450	0.1271020	0.1014960	0.0826264	0.0684094
0.6	0.2056680	0.1607330	0.1283580	0.1044970	0.0865184
0.7	0.2540680	0.1985680	0.1585770	0.1291010	0.1068910
0.8	0.3078470	0.2406070	0.1921530	0.1564380	0.1295270
0.9	0.3670030	0.2868500	0.2290870	0.1865100	0.1544270
1.0	0.4315370	0.3372960	0.2693790	0.2193150	0.1815910

5. Conclusions

FG elastic nano-rods under tension have been investigated by the modified nonlocal strain gradient (NSG) theory. The new formulation contains a nonlocal parameter and a material length scale parameter to incorporate the scaling effects of nonlocal stress and microstructure-dependent strain gradient. In comparison to other strain-driven methodologies, the new proposal has been shown to be well-posed and does not require higher-order boundary conditions. In fact, in addition to the classical static and kinematic boundary conditions, closure of the NSG model has to be carried out by prescribing suitable constitutive boundary conditions. Closed-form nonlocal solutions of FG clamped-free and clamped-clamped nano-rods have been provided, exhibiting stiffening or softening effects depending on the values of nonlocal and gradient parameters. Single-Walled Carbon Nanotubes (SWCNT) of armchair (10, 10) were modeled as NSG nano-rods, showing that the new approach could capture the small-scale behavior of Young’s modulus as predicted by the MD simulations. The nonlocal parameter was thus tuned to characterize Young’s modulus vs. the SWCNT length.

Author Contributions: Conceptualization, Methodology, Software, Validation, Investigation, Writing—Review & Editing: R.B., M.Č. and F.M.d.S. All the authors contributed equally to this work.

Funding: This research received no external funding.

Acknowledgments: Financial supports from the Italian Ministry of Education, University and Research (MIUR) in the framework of the Project PRIN 2015 “COAN 5.50.16.01”—code 2015JW9NJT—and from the research program ReLUIS 2018 are gratefully acknowledged.

Conflicts of Interest: The authors declare no conflict of interest.

Appendix A

The reduced stiffness can be alternatively obtained by considering a CC – δ nano-rod, which is a fully clamped nano-rod with an imposed axial displacement δ at the end point $x = L$.

Following the steps reported in Section 3, the axial force is expressed in terms of an unknown parameter in the form $N(x) = a_1$ so that the solution of the nano-rod is provided by the nonlocal differential equation

$$A_E \partial_x u(x) - l^2 A_E \partial_x^3 u(x) = a_1 \tag{A1}$$

under the CBC (Equation (26))

$$\begin{cases} \frac{a_1}{L_c} + \frac{l^2}{L_c^2} A_E \partial_x^2 u(x)|_{x=0} = 0 \\ -\frac{a_1}{L_c} + \frac{l^2}{L_c^2} A_E \partial_x^2 u(x)|_{x=L} = 0 \end{cases} \tag{A2}$$

and the classical boundary conditions (Equation (27))

$$\begin{cases} u(0) = 0 \\ u(L) = \delta. \end{cases} \tag{A3}$$

Hence, the axial displacement is

$$u(x) = u_e(x) + \frac{\delta L_c}{(e^{\frac{L}{l}} - 1) L (L + 2L_c)} e^{-\frac{x}{l}} \cdot [-e^{\frac{L}{l}} L + e^{\frac{2x}{l}} L + e^{\frac{L+x}{l}} (L - 2x) + e^{\frac{x}{l}} (2x - L)] \tag{A4}$$

where u_e is the axial displacement of the local model

$$u_e(x) = \frac{\delta}{L} x. \tag{A5}$$

Moreover, the value of the parameter a_1 provides the axial force

$$N(x) = \frac{A_E}{L + 2L_c} \delta \tag{A6}$$

and we recover the same value of the reduced stiffness reported in Equation (37).

References

1. Eringen, A.C. On differential equations of nonlocal elasticity and solutions of screw dislocation and surface waves. *J. Appl. Phys.* **1983**, *54*, 4703–4710. [CrossRef]
2. Peerlings, R.H.J.; Geers, M.G.D.; de Borst, R.; Brekelmans, W.A.M. A critical comparison of nonlocal and gradient-enhanced softening continua. *Int. J. Solids Struct.* **2001**, *38*, 7723–7746. [CrossRef]
3. Marotti de Sciarra, F.; Barretta, R. A new nonlocal bending model for Euler-Bernoulli nanobeams. *Mech. Res. Commun.* **2014**, *62*, 25–30. [CrossRef]
4. Askes, H.; Aifantis, E.C. Gradient elasticity in statics and dynamics: an overview of formulations, length scale identification procedures, finite element implementations and new results. *Int. J. Solids Struct.* **2011**, *48*, 1962–1990. [CrossRef]
5. Reddy, J.N. Nonlocal theories for bending, buckling and vibration of beams. *Int. J. Eng. Sci.* **2007**, *45*, 288–307. [CrossRef]
6. Barretta, R.; Marotti de Sciarra, F. Analogies between nonlocal and local Bernoulli–Euler nanobeams. *Arch. Appl. Mech.* **2015**, *85*, 89–99. [CrossRef]

7. Romano, G.; Barretta, R. Nonlocal elasticity in nanobeams: the stress-driven integral model. *Int. J. Eng. Sci.* **2017**, *115*, 14–27. [[CrossRef](#)]
8. Romano, G.; Barretta, R.; Diaco, M.; Marotti de Sciarra, F. Constitutive boundary conditions and paradoxes in nonlocal elastic nano-beams. *Int. J. Mech. Sci.* **2017**, *121*, 151–156. [[CrossRef](#)]
9. Barretta, R.; Diaco, M.; Feo, L.; Luciano, R.; Marotti de Sciarra, F.; Penna, R. Stress-driven integral elastic theory for torsion of nano-beams. *Mech. Res. Commun.* **2018**, *87*, 35–41. [[CrossRef](#)]
10. Barretta, R.; Čanadija, M.; Luciano, R.; Marotti de Sciarra, F. Stress-driven modeling of nonlocal thermoelastic behaviour of nanobeams. *Int. J. Eng. Sci.* **2018**, *126*, 53–67. [[CrossRef](#)]
11. Barretta, R.; Čanadija, M.; Feo, L.; Luciano, R.; Marotti de Sciarra, F.; Penna, R. Exact solutions of inflected functionally graded nano-beams in integral elasticity. *Compos. Part B* **2018**, *142*, 273–286. [[CrossRef](#)]
12. Barati, M.R. On wave propagation in nanoporous materials. *Int. J. Eng. Sci.* **2017**, *116*, 1–11. [[CrossRef](#)]
13. Fernández-Sáez, J.; Zaera, R. Vibrations of Bernoulli-Euler beams using the two-phase nonlocal elasticity theory. *Int. J. Eng. Sci.* **2017**, *119*, 232–248. [[CrossRef](#)]
14. Vila, J.; Fernández-Sáez, J.; Zaera, R. Nonlinear continuum models for the dynamic behavior of 1D microstructured solids. *Int. J. Solids Struct.* **2017**, *117*, 111–122. [[CrossRef](#)]
15. Xu, X.-J.; Zheng, M.-L.; Wang, X.-C. On vibrations of nonlocal rods: Boundary conditions, exact solutions and their asymptotics. *Int. J. Eng. Sci.* **2017**, *119*, 217–231. [[CrossRef](#)]
16. Faghidian, S.A. On non-linear flexure of beams based on nonlocal elasticity theory. *Int. J. Eng. Sci.* **2018**, *124*, 49–63. [[CrossRef](#)]
17. Faghidian, S.A. Integro-differential nonlocal theory of elasticity. *Int. J. Eng. Sci.* **2018**, *129*, 96–110. [[CrossRef](#)]
18. Sahmani, S.; Bahrami, M.; Ansari, R. Nonlinear free vibration analysis of functionally graded third-order shear deformable microbeams based on the modified strain gradient elasticity theory. *Compos. Struct.* **2014**, *110*, 219–230. [[CrossRef](#)]
19. Polizzotto, C.; Fuschi, P.; Pisano, A.A. A nonhomogeneous nonlocal elasticity model. *Eur. J. Mech. A/Solids* **2006**, *25*, 308–333. [[CrossRef](#)]
20. Fuschi, P.; Pisano, A.A.; Polizzotto, C. Size effects of small-scale beams in bending addressed with a strain difference based nonlocal elasticity theory. *Int. J. Mech. Sci.* **2019**, *151*, 661–671. [[CrossRef](#)]
21. Mindlin, R.D. Micro-structure in linear elasticity. *Arch. Ration. Mech. Anal.* **1964**, *16*, 51–78. [[CrossRef](#)]
22. Akgöz, B.; Civalek, Ö. Longitudinal vibration analysis of strain gradient bars made of functionally graded materials (FGM). *Compos. Part B* **2013**, *55*, 263–268. [[CrossRef](#)]
23. Rahaeifard, M. Size-dependent torsion of functionally graded bars. *Compos. Part B* **2015**, *82*, 205–211. [[CrossRef](#)]
24. Akgöz, B.; Civalek, Ö. Strain gradient elasticity and modified couple stress models for buckling analysis of axially loaded micro-scaled beams. *Int. J. Eng. Sci.* **2011**, *49*, 1268–1280. [[CrossRef](#)]
25. Ghayesh, M.H.; Farokhi, H.; Alici, G. Size-dependent performance of microgyroscopes. *Int. J. Eng. Sci.* **2016**, *100*, 99–111. [[CrossRef](#)]
26. Guo, J.; Chen, J.; Pan, E. Static deformation of anisotropic layered magneto-electroelastic plates based on modified couple-stress theory. *Compos. Part B* **2016**, *107*, 84–96. [[CrossRef](#)]
27. Lim, C.W.; Zhang, G.; Reddy, J.N. A higher-order nonlocal elasticity and strain gradient theory and its applications in wave propagation. *J. Mech. Phys. Solids* **2015**, *78*, 298–313. [[CrossRef](#)]
28. Fernandes, R.; El-Borgi, S.; Mousavi, S.; Reddy, J.; Mehmoum, A. Nonlinear size-dependent longitudinal vibration of carbon nanotubes embedded in an elastic medium. *Physica E* **2017**, *88*, 18–25. [[CrossRef](#)]
29. Guo, S.; He, Y.; Liu, D.; Lei, J.; Shen, L.; Li, Z. Torsional vibration of carbon nanotube with axial velocity and velocity gradient effect. *Int. J. Mech. Sci.* **2016**, *119*, 88–96. [[CrossRef](#)]
30. Li, L.; Hu, Y.; Li, X. Longitudinal vibration of size-dependent rods via nonlocal strain gradient theory. *Int. J. Mech. Sci.* **2016**, *115*, 135–144. [[CrossRef](#)]
31. Li, L.; Hu, Y.; Ling, L. Flexural wave propagation in small-scaled functionally graded beams via a nonlocal strain gradient theory. *Compos. Struct.* **2015**, *133*, 1079–1092. [[CrossRef](#)]
32. Simsek, M. Nonlinear free vibration of a functionally graded nanobeam using nonlocal strain gradient theory and a novel hamiltonian approach. *Int. J. Eng. Sci.* **2016**, *105*, 12–27. [[CrossRef](#)]
33. Shen, Y.; Chen, Y.; Li, L. Torsion of a functionally graded material. *Int. J. Eng. Sci.* **2016**, *109*, 14–28. [[CrossRef](#)]

34. Barati, M.R.; Zenkour, A. A general bi-helmholtz nonlocal strain-gradient elasticity for wave propagation in nanoporous graded double-nanobeam systems on elastic substrate. *Compos. Struct.* **2017**, *168*, 885–892. [[CrossRef](#)]
35. Li, L.; Hu, Y. Nonlinear bending and free vibration analyses of nonlocal strain gradient beams made of functionally graded material. *Int. J. Eng. Sci.* **2016**, *107*, 77–97. [[CrossRef](#)]
36. Ebrahimi, F.; Dabbagh, A. Wave dispersion characteristics of orthotropic double-nanoplatesystem subjected to a longitudinal magnetic field. *Microsyst. Technol.* **2018**, *24*, 2929–2939. [[CrossRef](#)]
37. Mirkalantari, S.A.; Hashemian, M.; Eftekhari, S.A.; Toghraie, D. Pull-in instability analysis of rectangular nanoplate based on strain gradient theory considering surface stress effects. *Physica B* **2017**, *519*, 1–14. [[CrossRef](#)]
38. Li, L.; Li, X.; Hu, Y. Free vibration analysis of nonlocal strain gradient beams made of functionally graded material. *Int. J. Eng. Sci.* **2016**, *102*, 77–92. [[CrossRef](#)]
39. Xu, X.J.; Wang, X.C.; Zheng, M.L.; Ma, Z. Bending and buckling of nonlocal strain gradient elastic beams. *Compos. Struct.* **2017**, *160*, 366–377. [[CrossRef](#)]
40. Zhu, X.; Li, L. Closed form solution for a nonlocal strain gradient rod in tension. *Int. J. Eng. Sci.* **2017**, *119*, 16–28. [[CrossRef](#)]
41. Xu, X.-J.; Zhou, B.; Zheng, M.-L. Comment on “Free vibration analysis of nonlocal strain gradient beams made of functionally graded material” [*Int. J. Eng. Sci.* **2016**, *102*, 77–92]. *Int. J. Eng. Sci.* **2017**, *119*, 189–191. [[CrossRef](#)]
42. Barretta, R.; Marotti de Sciarra, F. Constitutive boundary conditions for nonlocal strain gradient elastic nano-beams. *Int. J. Eng. Sci.* **2018**, *130*, 187–198. [[CrossRef](#)]
43. Apuzzo, A.; Barretta, R.; Faghidian, S.A.; Luciano, R.; Marotti de Sciarra, F. Free vibrations of elastic beams by modified nonlocal strain gradient theory. *Int. J. Eng. Sci.* **2018**, *133*, 99–108. [[CrossRef](#)]
44. Duan, K.; Li, L.; Hu, Y.; Wang, X. Enhanced interfacial strength of carbon nanotube/copper nanocomposites via Ni-coating: Molecular-dynamics insights. *Physica E* **2017**, *88*, 259–264. [[CrossRef](#)]
45. Vodenitcharova, T.; Zhang, L.C. Effective wall thickness of a single-walled carbon nanotube. *Phys. Rev. B* **2003**, *68*, 165401. [[CrossRef](#)]
46. De Domenico, D.; Askes, H. Stress gradient, strain gradient and inertia gradient beam theories for the simulation of flexural wave dispersion in carbon nanotubes. *Compos. Part B* **2018**, *153*, 285–294. [[CrossRef](#)]
47. De Domenico, D.; Askes, H. Nano-scale wave dispersion beyond the First Brillouin Zone simulated with inertia gradient continua. *J. Appl. Phys.* **2018**, *124*, 205107. [[CrossRef](#)]



© 2019 by the authors. Licensee MDPI, Basel, Switzerland. This article is an open access article distributed under the terms and conditions of the Creative Commons Attribution (CC BY) license (<http://creativecommons.org/licenses/by/4.0/>).